

Polyhedral vesicles

Hiroshi Noguchi*

Department of Theoretical Studies, Institute for Molecular Science Okazaki 444-8585, Japan

Polyhedral vesicles with a large bending modulus of the membrane such as the gel phase lipid membrane were studied using a Brownian dynamics simulation. The vesicles exhibit various polyhedral morphologies such as tetrahedron and cube shapes. We clarified two types of line defects on the edges of the polyhedrons: cracks of both monolayers at the spontaneous curvature of monolayer $C_0 < 0$, and a crack of the inner monolayer at $C_0 \geq 0$. Around the latter defect, the inner monolayer curves positively. Our results suggested that the polyhedral morphology is controlled by C_0 .

PACS numbers: 87.16.Dg, 87.16.Ac, 82.70.Uv

Amphiphilic molecules such as lipids and detergents form various structures such as micelles, cylindrical structures, and bilayer membranes in aqueous solution [1]. In particular, closed bilayer membranes, i.e., vesicles, are biologically important as model systems for the plasma membrane and intracellular compartments in living cells. Various morphological changes in the vesicles are understood via the Helfrich elastic model [1, 2, 3]. However, this model can not be applied to non-bilayer structures. For example, in an inverted hexagonal H_{II} phase, the hydrophobic interstice (void) space opens among three cylindrical monolayers. Recently, it is considered that this interstice space is filled by the tilt deformation of amphiphilic molecules as shown in Fig. 1(a) [4]. The molecules tilt with respect to the monolayer surfaces around the junction of the three bilayers. The monolayer surfaces are sharply bent at the junction. The effects of tilt deformation are also studied regarding the fusion intermediates of fluid phase membranes [5].

On the other hand, polyhedral-shaped vesicles of μm scale size were observed in the gel phase; a triangular pyramid or prism-shaped vesicle of a mono-component lipid [6], and an icosahedral vesicle of mixtures of cationic and anionic surfactants [7]. The membranes are flat on the faces of polyhedrons and are sharply bent at the edges. Because the bending modulus are very large in the gel phase, the polyhedral vesicles would be stabler than the spherical vesicles. The free-energy loss of the defects at the edges would be less than the loss of the equal bending of membranes on the sphere. However, the defect structure at the edges is unresolved. The information of the edge structure is significant to control the morphology of the polyhedral vesicles. These vesicles are expected to be of practical value for drug delivery.

To clarify the edge structure, theories or simulations with molecular resolution are needed. Since molecular dynamics simulations with atomic resolution have been applied only for the $\sim 10\text{ns}$ dynamics of 1000 lipid molecules due to the restrictions of computational time [8], coarse-grained molecular simulations [9, 10, 11, 12, 13] have been applied. We studied the fusion and fission dynamics of vesicles using Brownian dynam-

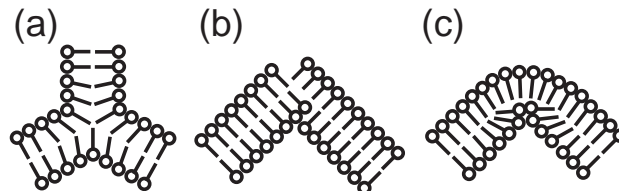


FIG. 1: Three types of Line defects. (a) Tilt deformation in the inverted hexagonal phase. (b) Cracks of both monolayers. Hydrophobic segments are partially exposed. (c) Crack of inner monolayer. Amphiphilic molecules in the inner monolayer tilt with respect to the boundary surfaces of two monolayers.

ics [11]. The self-assembly into vesicles is simulated by our model [10], a lattice Monte Carlo method [12], and dissipative particle dynamics [13]. However, these simulated vesicles were flexible, and no polyhedral vesicle has been obtained.

In the present paper, we developed our previous model to control the bending modulus of monolayers by the addition of the curvature potential of a monolayer. We simulated the polyhedral vesicles of rigid membranes, and obtained two types of defects at the edges as shown in Figs. 1(b) and (c). The morphology of the polyhedral vesicles and the defect type depend on the spontaneous curvature of the monolayer C_0 .

An amphiphilic molecule is modeled as rigid rods consisting of one hydrophilic segment ($j = 1$) and two hydrophobic segments ($j = 2, 3$), which are separated by a fixed distance σ . Solvent molecules are not explicitly taken into account, and “hydrophobic” interaction is mimicked by the multibody local density potential of the hydrophobic segments. As details of the basic model were described in our previous papers [10, 11], here we briefly explain the model. The motion of the j th segment of the i th molecule follows the underdamped Langevin equation. Amphiphilic molecules ($i = 1, \dots, N$) interact via a repulsive soft-core potential U_{rep} , an attractive “hydrophobic” potential U_{hp} , and a curvature potential U_{CV} .

$$U = \sum_{i \neq i'} U_{\text{rep}}(|\mathbf{r}_{i,j} - \mathbf{r}_{i',j'}|) + \sum_{j=2,3} U_{\text{hp}}(\rho_{i,j}) + U_{\text{CV}}, \quad (1)$$

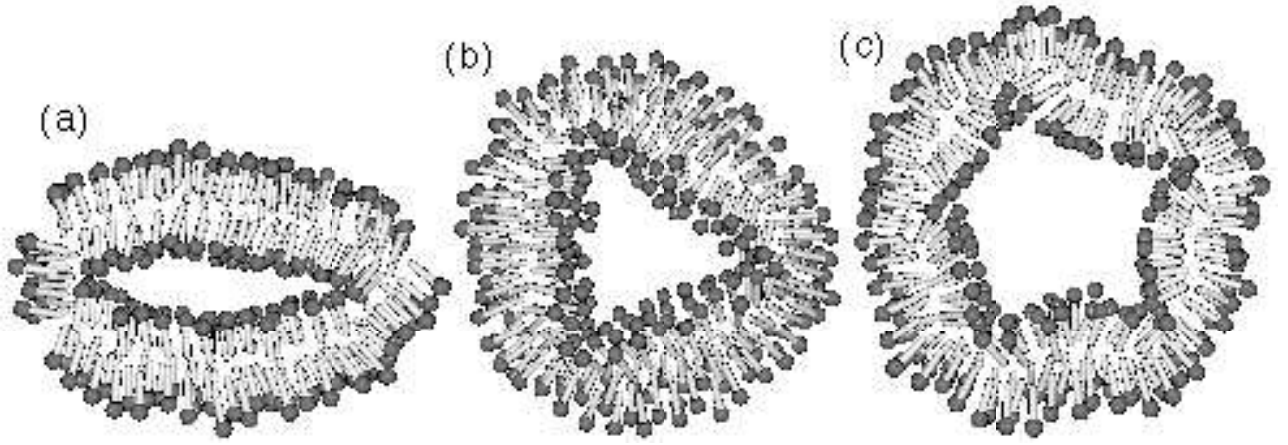


FIG. 2: Sliced snapshots of vesicles at temperature $k_B T/\varepsilon = 0.2$ and the number of molecules $N = 1000$. (a) Disk shaped (dihedral) vesicle at the spontaneous curvature of monolayer $C_0\sigma = -0.11$. (b) Triangular-pyramid shaped (tetrahedral) vesicle at $C_0\sigma = 0.058$. (c) Pentagonal-prism shaped (septihedral) vesicle at $C_0\sigma = 0.23$. Gray spheres and white cylinders represent hydrophilic and hydrophobic segments of amphiphilic molecules, respectively.

where $\rho_{i,j}$ is the local density of the hydrophobic segments for the j th segment of the i th molecule. Both segments have the same soft radius, $U_{\text{rep}}(r)/\varepsilon = \exp\{-20(r/\sigma - 1)\}$. The “hydrophobic” interaction is mimicked by the potential $U_{\text{hp}}(\rho)$.

$$\rho_{i,j} = \sum_{i \neq i', j'=2,3} h(|\mathbf{r}_{i,j} - \mathbf{r}_{i',j'}|), \quad (2)$$

$$\text{where } h(r) = \frac{1}{\exp\{20(r/\sigma - 1.9)\} + 1}.$$

$\rho_{i,j}$ is the number of hydrophobic segments in the sphere whose radius is approximately 1.9σ .

$$U_{\text{hp}}(\rho)/\varepsilon = \begin{cases} -0.5\rho & (\rho < \rho^* - 1) \\ 0.25(\rho - \rho^*)^2 - c & (\rho^* - 1 \leq \rho < \rho^*) \\ -c & (\rho^* \leq \rho) \end{cases}, \quad (3)$$

where c is given by $c = 0.5\rho^* - 0.25$. We used the values $\rho^* = 10$ and 14 at $j = 2$ and 3 , respectively.

To give the bending modulus κ and the spontaneous curvature C_0 of the monolayer membranes, we use the potential U_{CV} of the orientational difference of neighboring molecules.

$$U_{\text{CV}} = \sum_{i \neq i'} 0.5\kappa'_{\text{cv}} h(r_{i,i'}) (\mathbf{u}_i - \mathbf{u}_{i'} - C'_0 \hat{\mathbf{r}}_{i,i'})^2, \quad (4)$$

where the vector \mathbf{u}_i is the unit orientational vector of the i th molecule, and $\hat{\mathbf{r}}_{i,i'}$ ($r_{i,i'}$) is the unit vector (distance) between the i th and i' th molecules: $\mathbf{u}_i = (\mathbf{r}_{i,1} - \mathbf{r}_{i,3})/|\mathbf{r}_{i,1} - \mathbf{r}_{i,3}|$ and $\hat{\mathbf{r}}_{i,i'} = (\mathbf{r}_i - \mathbf{r}_{i'})/|\mathbf{r}_i - \mathbf{r}_{i'}|$, where \mathbf{r}_i is the center of mass of the i th molecule. At $C'_0 = 0$, this potential is similar to the bending elastic potential used in the tethered membrane models [14]. When the

orientational vectors \mathbf{u}_i are equal to the normal vectors of the monolayers with no tilt deformation,

$$U_{\text{CV}}/\varepsilon = \int 0.5\kappa'_{\text{cv}} [(C_1 + C_2 - C_0)^2 - 2C_1C_2 + C_0^2] dA \quad (5)$$

in the continuum limit, where C_1 and C_2 are the two principal curvatures of a monolayer. The spontaneous curvature C_0 equals to $C'_0\sigma/\bar{r}_{\text{nb}}$, where \bar{r}_{nb} is the mean distance between neighboring molecules and $\bar{r}_{\text{nb}} = 1.5\sigma$. On the assumption of the hexagonal packing of molecules in the monolayers, we obtain $\kappa'_{\text{cv}} = \sqrt{3}\kappa'_{\text{cv}}$. We used $\kappa'_{\text{cv}} = 3\varepsilon$ to represent the rigid membrane, and $\kappa'_{\text{cv}} \simeq 5\varepsilon$. In previous papers, we estimated the bending modulus $\kappa_0/\varepsilon \simeq 0.5$ (half of the bending modulus of bilayers) at $\kappa'_{\text{cv}} = 0$ [11]. Since κ_{cv} is ten times larger than κ_0 , the bending elasticity is mainly given by U_{CV} , and the bending modulus of the monolayer $\kappa \simeq \kappa_{\text{cv}}$.

We mainly used the number of molecules $N = 1000$ and $k_B T/\varepsilon = 0.2$, where k_B is the Boltzmann constant and T is the temperature. Amphiphilic molecules spontaneously form vesicles in a fluid phase at $k_B T/\varepsilon = 0.2$ and $\kappa'_{\text{cv}} = 0$. The unit length σ corresponds to $\sim 1\text{nm}$. The unit time step $\tau_0 = \zeta\sigma^2/\varepsilon$ corresponds to $\sim 1\text{ns}$ estimated from the lateral diffusion constant of phospholipid at 30°C , $\sim 10^{-7}\text{cm}^2/\text{s}$ [15], where ζ is the friction constant of the segments of molecules.

Vesicles exhibit various polyhedral morphologies at $\kappa'_{\text{cv}} = 3\varepsilon$. The number of faces n_f of polyhedron increases as C_0 increases. Figure 2 shows examples of the polyhedral vesicles. The edges of the polyhedrons are formed by the line defects [Figs. 1(b) and (c)]. The molecules at the line defects are shown using the number of neighboring molecules n_i^{nb} in Fig. 3. The inner monolayers are divided into n_f faces by the defects. At $C_0 \geq 0$, the cracks of the inner monolayer [Fig. 1(c)] occur on the edges, and the outer monolayer consists of one curved



FIG. 3: Line defects (edges) of the tetrahedral vesicle in Fig. 2(b). The snapshot is viewed from the same viewpoint. The molecules with number of neighboring molecules $n_i^{\text{nb}} < 4.5$ in the inner monolayer are shown. The number n_i^{nb} is defined as $n_i^{\text{nb}} = \sum h(r_{i,i'})$.

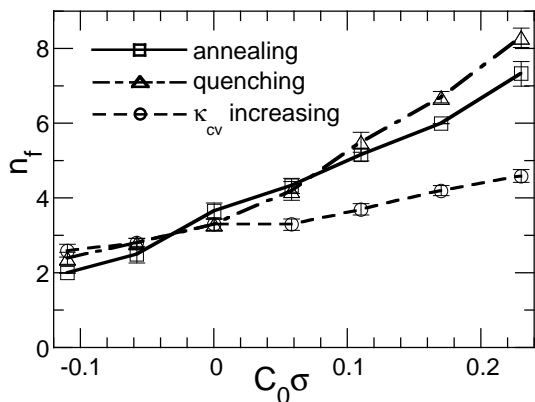


FIG. 4: Spontaneous curvature C_0 dependence of the mean number of faces $\langle n_f \rangle$ of polyhedrons at $N = 1000$ and $k_B T/\varepsilon = 0.2$. Annealing: Vesicles are annealed from $k_B T/\varepsilon = 0.5$ to 0.2. Quenching: Vesicles are simulated starting with spherical vesicles at $\kappa'_{cv} = 0$. κ'_{cv} increasing: the coefficient κ'_{cv} slowly increases from $\kappa'_{cv}/\varepsilon = 0$ to 3 starting with the spherical vesicles at $\kappa'_{cv} = 0$.

face [Figs. 2(b) and (c)]. At $C_0 < 0$, the outer monolayer also exhibits cracks [Fig. 1(b)] on the edges. When the deformation of the left or right side of Fig. 2(a) is formed on the entire circular-line defects, the outer monolayer of the disk-shaped vesicles is divided into three faces (two disks and one cylinder) or two faces, respectively.

Figure 4 shows the mean number of faces $\langle n_f \rangle$ at $k_B T/\varepsilon = 0.2$ using three methods. The results of annealing are the closest to the equilibrium values. Through the other methods, however, vesicles are often trapped in metastable states. At $C_0 > 0$, vesicles with larger (smaller) n_f values are obtained through quenching (κ'_{cv} increasing) than through annealing. Thus, one should use the annealing method to obtain regular polyhedrons.

Flip-flop motion, which is the transverse motion between the inner and outer monolayers, frequently occurs at $k_B T/\varepsilon = 0.5$. The number of molecules in the inner monolayer decreases with an increase in n_f at

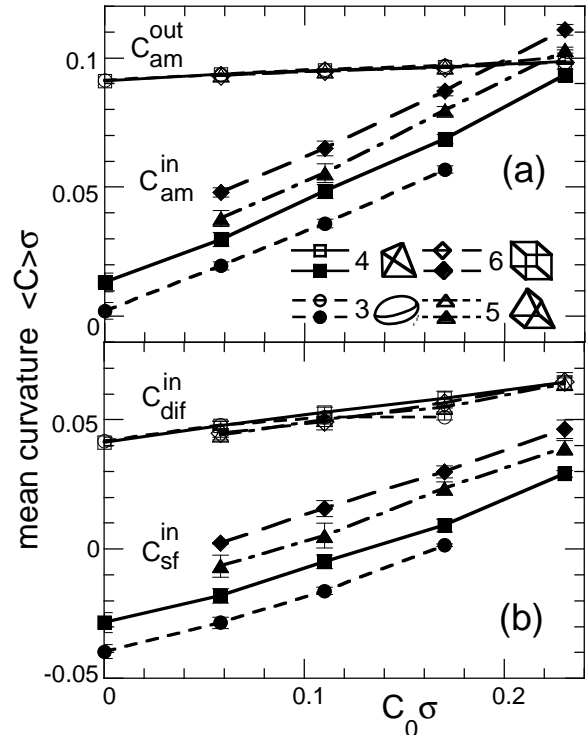


FIG. 5: Spontaneous curvature C_0 dependence of (a) the mean curvature for amphiphilic molecules, $\langle C_{am} \rangle$ (b) the mean curvature for monolayer surface $\langle C_{sf} \rangle$ and the difference $\langle C_{dif} \rangle = \langle C_{am} - C_{sf} \rangle$ at $N = 1000$, $k_B T/\varepsilon = 0.2$, and $\gamma_{in} = 0.328(\pm 0.003)$. The superscripts 'in' and 'out' represent inner and outer monolayers, respectively. Circles: rugby-ball shaped trihedron. Squares: tetrahedron. Triangles: triangular prism. Diamonds: cube.

$k_B T/\varepsilon = 0.5$, since tilting molecules on the line defects share a larger area. The ratios γ_{in} of molecules in the inner monolayer are $0.31(\pm 0.01)$ and $0.292(\pm 0.003)$ at $C_0 \sigma = -0.11$ ($n_f = 2$) and $C_0 \sigma = 0.23$ ($n_f = 7.3$), respectively. On the other hand, flip-flop motion rarely occurs, and the ratio γ_{in} is fixed at $\gamma_{in} = 0.328(\pm 0.003)$ at the fixed temperature $k_B T/\varepsilon = 0.2$. In typical experimental conditions, flip-flop motion is very slow, and the half-life is more than several hours even in the fluid phase [16]. Thus experimentally, the ratio γ_{in} of the polyhedral vesicles should not reach an equilibrium value as well as the simulation with the fixed temperature $k_B T/\varepsilon = 0.2$.

In the obtained polyhedrons, three edges are connected at any vertex. The connections of more edges are unstable and are not formed. The number of edges n_e then equals to 1.5 times the number of vertices n_v , because each edge contacts two vertices. We derived $n_e = 3(n_f - 2)$ and $n_v = 2(n_f - 2)$ from this relation and Euler's formula for a convex polyhedron ($n_f + n_v - n_e = 2$). At $n_f \geq 6$, multiple types of polyhedrons with the same number of faces exist. However, we obtained only one or two types of polyhedrons; i.e., cube (4^6) at $n_f = 6$; pentagonal prism ($4^5, 5^2$) and ($3^1, 4^3, 5^3$) at $n_f = 7$; ($4^4, 5^4$)

at $n_f = 8$; ($4^3, 5^6$) and ($4^4, 5^4, 6^1$) at $n_f = 9$, where (p^q) represents a polyhedron with q p -gons. Thus more symmetric polyhedrons are more frequently formed.

Figure 5(a) shows the C_0 dependence of the curvatures of four polyhedrons at $C_0 \geq 0$, where C_{am} is the curvature (splay) for amphiphilic molecules, $\langle C_{\text{am}} \rangle = \bar{r}_{\text{nb}} = (\sum(\mathbf{u}_i - \mathbf{u}_{i'})\hat{\mathbf{r}}_{i,i'}h(r_{i,i'}))/(\sum h(r_{i,i'}))$. The mean curvature $\langle C_{\text{am}}^{\text{out}} \rangle$ of the outer monolayer is almost independent of C_0 and n_f . On the other hand, $\langle C_{\text{am}}^{\text{in}} \rangle$ of the inner monolayer increases with an increase in C_0 and n_f , since the inner monolayers curve positively around the crack of the inner monolayers. The mean curvature $\langle C_{\text{am}}^{\text{in}} \rangle$ for a larger n_f is closer to C_0 , though more hydrophilic segments contact the hydrophobic segments at the line defects. The curvature C_{am} does not coincide with the curvature of the monolayers, since molecules can tilt with respect to the monolayer surface. To clarify this tilt, we estimated the curvature C_{sf} for the monolayer surface, $\langle C_{\text{sf}} \rangle = \bar{r}_{\text{nb}} = (\sum(\mathbf{n}_i - \mathbf{n}_{i'})\hat{\mathbf{r}}_{i,i'}h(r_{i,i'}))/(\sum h(r_{i,i'}))$, where \mathbf{n}_i is the normal vector of the monolayer surface at \mathbf{r}_i . We defined \mathbf{n}_i as the vector minimizing $\varepsilon_i = \sum h(r_{i,i'}) (\mathbf{n}_i \hat{\mathbf{r}}_{i,i'})^2$ when $n_i^{\text{nb}} > 2.5$. This minimizing vector is the eigenvector with the smallest eigenvalue of the moment tensor of inertia of the neighboring molecules. Figure 5(b) shows the curvatures $\langle C_{\text{sf}}^{\text{in}} \rangle$ of the inner monolayer surface and difference $\langle C_{\text{dif}}^{\text{in}} \rangle$ between the two curvatures. The inner monolayer surface (molecules in the inner monolayer) tilt with respect to the boundary surfaces of the two monolayers (the inner monolayer). Both tilts increase C_{am} . Since the molecular tilt in the inner monolayer $\langle C_{\text{dif}}^{\text{in}} \rangle$ is almost independent of n_f , the length of the line defects only changes the curvature $\langle C_{\text{sf}}^{\text{in}} \rangle$ of the inner monolayer surface. Thus the polyhedral morphology at equilibrium should be determined by the effects of line defects on $\langle C_{\text{sf}}^{\text{in}} \rangle$ and the hydrophobic interaction.

We found that the spontaneous curvature C_0 can be estimated using this tilt deformation with respect to the monolayer surface. At $C_{\text{sf}} < C_0$ ($C_{\text{sf}} > C_0$), molecules tilt to reduce $|C_{\text{am}} - C_0|$ and C_{dif} shows a positive (negative) value. Thus, we estimate $C_0\sigma \simeq 0.04$ at $\kappa'_{\text{cv}} = 0$ and $k_{\text{B}}T/\varepsilon = 0.2$: $\langle C_{\text{dif}} \rangle = \sigma = 0.0041(\pm 0.0002)$ for flat membranes; $\langle C_{\text{dif}}^{\text{out}} \rangle = \sigma = 0.0(\pm 0.00007)$ and $\langle C_{\text{sf}}^{\text{out}} \rangle = \sigma = 0.0429(\pm 0.0005)$ for tube-shaped vesicles with a diameter of 30σ ; and $\langle C_{\text{dif}}^{\text{out}} \rangle = \sigma = -0.0056(\pm 0.0003)$ and $\langle C_{\text{sf}}^{\text{out}} \rangle = \sigma = 0.0975(\pm 0.0003)$ for spherical vesicles with a diameter of 20σ .

The line defects may be interpreted using the correction terms of the Helfrich model, the local minimum at a large $C_1 + C_2$. The morphology of the polyhedral vesicles may then be obtained from the Euler-Lagrange differential equation. Similar deformations to the crack of the inner monolayer are seen in our daily experience. When a rubber hose is strongly bent, a side of the hose becomes hollow, and the other side smoothly bends.

The morphology of the polyhedral vesicles depends on

the number N and properties of molecules. At $N = 2000$ and $C_0\sigma = 0.23$, vesicles exhibit more complex morphologies with concave edges, where the membrane bends outside with a crack of the outer monolayer. The hexagonal packing of molecules should stabilize the triangular and hexagonal faces. In some multi-component vesicles, the phase separation occurs at the edges or vertices of the polyhedrons. Dubois *et al.* reported that the segregated anionic surfactants form pores at the vertices [7]. Various polyhedral vesicles are likely to be experimentally observed under the control of C_0 and other conditions.

This work was supported in part by a Grant-in-Aid for Scientific Research from the Ministry of Education, Culture, Sports, Science, and Technology of Japan.

* noguchi@ims.ac.jp

- [1] *Structure and Dynamics of Membranes* edited by R. Lipowsky and E. Sackmann (Elsevier Science, Amsterdam, 1995); S. A. Safran, *Statistical Thermodynamics of Surfaces, Interfaces, and Membranes* (Addison-Wesley, New York, 1994).
- [2] W. Helfrich, Z. Naturforsch **28c**, 693 (1973).
- [3] U. Seifert, Adv. Phys. **46**, 13 (1997).
- [4] M. Hamm and M. M. Kozlov, Eur. Phys. J. B **6**, 519 (1998).
- [5] P. I. Kuzmin, J. Zimmerberg, Yu. A. Chizmadzhev, and F. S. Cohen, Proc. Natl. Acad. Sci. USA **98**, 7235 (2001); Y. Kozlovsky and M. M. Kozlov, Biophys. J. **82**, 882 (2002).
- [6] E. Sackmann, FEBS lett. **346**, 3 (1994).
- [7] M. Dubois *et al.*, Nature **411**, 672 (2001).
- [8] L. R. Forrest and M. S. P. Sansom, Curr. Opin. Struct. Biol. **10**, 174 (2000); S. E. Feller, Curr. Opin. Colloid Interface Sci. **5**, 217 (2000); S. J. Marrink, E. Lindahl, O. Edholm, and A. E. Mark, J. Am. Chem. Soc. **123**, 8638 (2001).
- [9] S. Karaborni *et al.*, Science **266**, 254 (1994); R. Goetz, G. Gompper, and R. Lipowsky, Phys. Rev. Lett. **82**, 221 (1999); T. Soddemann, B. Dünweg, and K. Kremer, Eur. Phys. J. E **6**, 409 (2001); R. D. Groot and K. L. Rabone, Biophys. J. **81**, 725 (2001).
- [10] H. Noguchi and M. Takasu, Phys. Rev. E **64**, 041913 (2001).
- [11] H. Noguchi and M. Takasu, J. Chem. Phys. **115**, 9547 (2001); Biophys. J. **83**, 299 (2002); Phys. Rev. E **65**, 051907 (2002); H. Noguchi, J. Chem. Phys. (2002) in press.
- [12] A. T. Bernardes, J. Phys. II **6**, 169 (1996).
- [13] S. Yamamoto, Y. Maruyama, and S. -a. Hyodo, J. Chem. Phys. **116**, 5842 (2002).
- [14] H. S. Seung and D. R. Nelson, Phys. Rev. A **38**, 1005 (1988); G. Gompper and D. M. Kroll, Phys. Rev. E **51**, 514 (1995).
- [15] E.-S. Wu, K. Jacobson, and D. Papahadjopoulos, Biochemistry **16**, 3936 (1977); W. Pfeiffer *et al.*, Europhys. Lett. **8**, 201 (1989).
- [16] R. D. Kornberg and H. M. McConnell, Biochemistry **10**, 1111 (1971); P. F. Devaux, Biochemistry **30**, 1163 (1991).

